Thermochimica Acta, 43 (1981) 91—102
Elsevier Scientific Publishing Company, Amsterdam — Printed in Belgium

REACTIVITY OF AMORPHOUS ALUMINAS PREPARED BY THE THERMAL DECOMPOSITION OF ALUMINUM CHLORIDE AND NITRATE

TAKESHI TSUCHIDA, AKIHIRO SAKATA, RYUSABURO FURUICHI and TADAO ISHII

Department of Applied Chemistry, Faculty of Engineering, Hokkaido University, Sapporo 060 (Japan)

(Received 25 June 1980)

ABSTRACT

The physicochemical properties and reactivity of amorphous aluminas, Al_2O_3(Cl) and Al_2O_3(N), which were prepared by the thermal decomposition of $AlCl_3 \cdot 6\,H_2O$ and $Al(NO_3)_3 \cdot 9\,H_2O$ at 600°C for 2—300 h, were investigated by means of TG, DTA, X-ray diffraction, SEM and IR. The reactivity of Al_2O_3(Cl) for $ZnAl_2O_4$ formation was, in general, higher than that of Al_2O_3(N) and was influenced by the content of residual chlorine in Al_2O_3(Cl). The rate of $ZnAl_2O_4$ formation followed the Avrami—Erofeev equation in the ZnO—Al_2O_3(Cl) system and the Jander equation in the ZnO—Al_2O_3(N) system, respectively.

INTRODUCTION

It has already been reported [1—3] that amorphous alumina forms in the course of the thermal decomposition of $AlCl_3 \cdot 6\,H_2O$ and $Al(NO_3)_3 \cdot 9\,H_2O$ and crystallizes to η- or γ-Al_2O_3 at around 800°C. Very few papers, however, have been reported on the structure, properties and reactivity of amorphous alumina, probably because of the lack of excellent means of investigating amorphous solids.

The object of the present study is to investigate the physicochemical properties of amorphous aluminas, Al_2O_3(Cl) and Al_2O_3(N), prepared by the thermal decomposition of $AlCl_3 \cdot 6\,H_2O$ and $Al(NO_3)_3 \cdot 9\,H_2O$ and to discuss the difference in their reaction behavior and reactivity for $ZnAl_2O_4$ formation. The influence of the chlorine content of Al_2O_3(Cl) on the reactivity is also described.

EXPERIMENTAL

Amorphous alumina samples were prepared by the thermal decomposition of $AlCl_3 \cdot 6\,H_2O$ and $Al(NO_3)_3 \cdot 9\,H_2O$ in a stream of air (100 ml min^{-1}) at 600°C for various times (2—300 h), which are called hereafter the prepara-

0040-6031/81/0000—0000/$02.50

tion times. Zinc oxide was obtained by the thermal decomposition of basic zinc carbonate, $5\,ZnO \cdot 2\,CO_3 \cdot 4\,H_2O$, at 550°C for 30 min. All samples were sieved to obtain — 300 mesh fraction.

X-Ray diffraction analysis was carried out with Geigerflex 2141 type (Rigaku Denki Co.) under the following conditions: Cu-target, Ni-filter, 25 kV, 10 mA, 2°C min^{-1}, 1 sec-time constant and 1°, 1°, 0.3 mm slit system. The conditions were replaced by 0.5°C min^{-1} and 4 sec-time constant for the determination of the lattice constant and crystallite size of $ZnAl_2O_4$, with silicon as an internal standard.

The weight loss of amorphous aluminas was measured by the simultaneous TG—DTA Model 8085 thermoanalyzer (Rigaku Denki Co.) in static air at a heating rate of 10°C min^{-1} up to 1300°C.

Scanning electron microscopy was carried out with a Hitachi-Akashi Model MSM4 SEM. The samples were mounted on aluminum stubs with double-sided cellulose tape and were coated with a sputtering-deposited gold film.

Infrared spectra were taken by the KBr disk method with a Digilab FTS Model 15 Fourier-transform IR spectrophotometer. The intensity of spectra was integrated 1000 times over the range 4000—400 cm^{-1}.

After a sample was degassed with a vacuum pump at 200°C for 1 h (air pressure was about 10^{-4} mm Hg), the specific surface area was determined by measuring nitrogen adsorption at —196°C. Pycnometric density measurement was carried out using water after the evacuation of samples by an aspirator for 10 min.

In order to determine the electrical conductivity of amorphous aluminas, a pellet 10 cm in diameter was obtained by compressing alumina (ca. 150 mg) at 300 kg cm^{-2} for 30 min and both sides of it were coated with a sputtering-deposited gold film ca. 500 Å thick. The aluminum foil electrode was joined to each surface of the pellet with silver paste and was further connected to copper wire. The pellet was then introduced into the furnace kept at a desired temperature and the conductivity was determined from measuring the resistivity by using a TOA Electronics Co. Super-Megohmmeter SM9. About 15—60 min elapsed before the resistivity became constant.

In order to determine the chlorine content of Al_2O_3(Cl), the alumina sample (ca. 100—200 mg) was dissolved in 1 M $NaHSO_4$ solution (50 ml) at 65°C for 2 h and the chlorine content in the solution was measured by colorimetric titration [4] using mercuric thiocyanate, $Hg(SCN)_2$, and ferric ammonium sulfate, $Fe_2(SO_4)_3 \cdot (NH_4)_2SO_4 \cdot 24\,H_2O$. Under the dissolution conditions mentioned above, the alumina samples of the preparation times longer than 75 h left a small amount of insoluble residue, which was removed by filtration.

Samples used in $ZnAl_2O_4$ formation were prepared in an agate mortar by mixing amorphous alumina with zinc oxide in an equimolar ratio. In the case of the isothermal experiments, the mixture (ca. 70 mg) was taken in a porcelain boat and was then allowed to react in an electrical furnace at a given temperature for a given time. In the DTA experiments, the ZnO—Al_2O_3 mixture (ca. 190 mg) or alumina alone (ca. 150 mg) was taken in a platinum holder and heated to 1300°C at 10°C min^{-1} in static air with a Model 8001

DTA (Rigaku Denki Co.). In order to analyze the samples in the course of DTA runs, the samples heated to various temperatures were taken out of the furnace, quenched to room temperature and were then subjected to X-ray diffraction and chemical analysis. Fractional formation of $ZnAl_2O_4(\alpha)$ was calculated from the difference between the amounts of ZnO in the samples before and after the reaction. The amount of ZnO was estimated from that of Zn^{2+} which was extracted from the sample with NH_4Cl—NH_4OH solution. The concentration of Zn^{2+} in the solution was determined with 0.01 M EDTA standard solution. All reagents used in this experiment were of GR grade and were supplied by Kanto Chemical Co., Inc.

RESULTS AND DISCUSSION

Preparation of amorphous aluminas and their properties

Table 1 shows the specific surface area, density and chlorine content of amorphous aluminas, Al_2O_3(Cl) and Al_2O_3(N), which were prepared by the thermal decomposition of $AlCl_3 \cdot 6\,H_2O$ and $Al(NO_3)_3 \cdot 9\,H_2O$ at 600°C for various preparation times. The symbols Cl and N in parentheses attached to Al_2O_3 in the first column of Table 1 represent aluminum chloride and nitrate used as starting materials and the number indicates the preparation time (h). Although the X-ray patterns of Al_2O_3(Cl, 250) and Al_2O_3(Cl, 300) gave faint and diffuse diffraction lines around $2\theta = 46°$ and 67° which probably correspond to η-Al_2O_3, other samples showed no X-ray peak and thus were confirmed to be in an amorphous state. As shown in Table 1, the specific surface area and the density of Al_2O_3(Cl) are nearly constant and independent of the preparation time, while the chlorine content decreases with increasing

TABLE 1

Properties of amorphous aluminas prepared by the thermal decomposition of $AlCl_3 \cdot 6H_2O$ and $Al(NO_3)_3 \cdot 9H_2O$ at 600°C for various times in flowing air (100 ml min^{-1})

Samples [a]	Surface area ($m^2\ g^{-1}$)	Density ($g\ cm^{-3}$)	Cl content (wt.%)
Al_2O_3(Cl, 2)	146		3.4
Al_2O_3(Cl, 5)	145	2.6	2.4
Al_2O_3(Cl, 10)	148		1.7
Al_2O_3(Cl, 25)	146	2.6	1.5
Al_2O_3(Cl, 50)	141		1.2
Al_2O_3(Cl, 75)	145		1.0
Al_2O_3(Cl, 100)	141		0.9
Al_2O_3(Cl, 150)	138	2.6	1.0
Al_2O_3(Cl, 250)	136		0.7
Al_2O_3(Cl, 300)	144		0.3
Al_2O_3(N, 2)	108	2.6	

[a] Cl and N in parentheses represent aluminum chloride and nitrate used as starting materials, and the number is the preparation time (h).

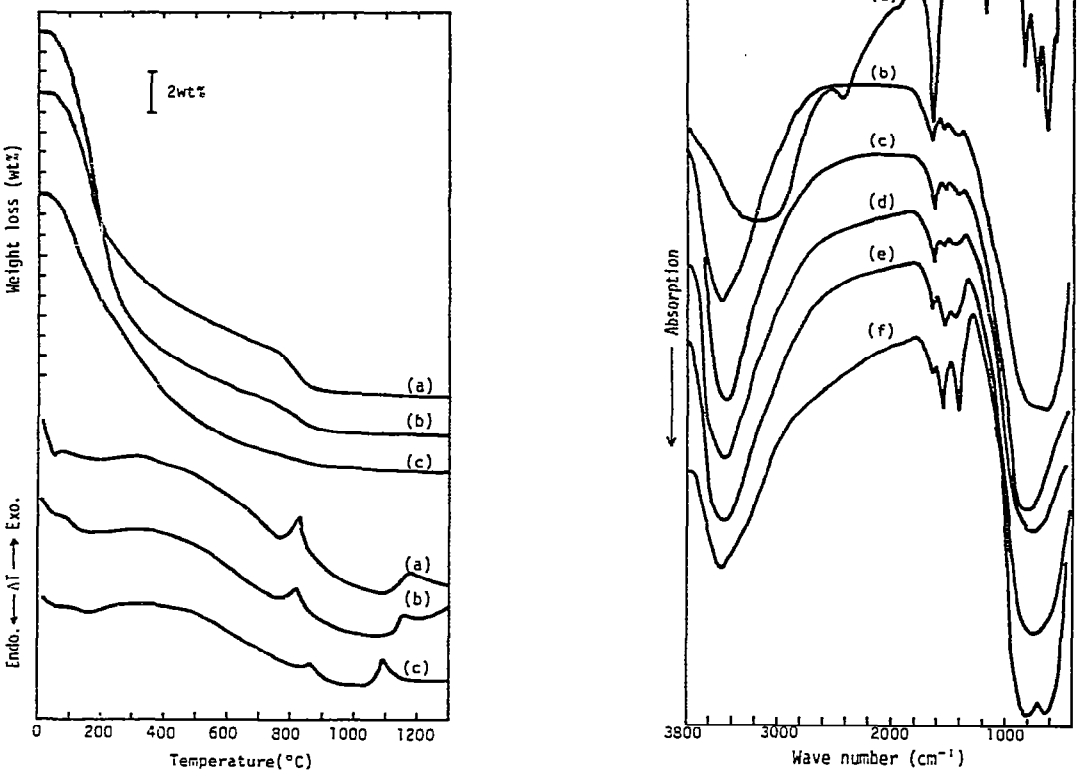

Fig. 1. TG and DTA curves of amorphous aluminas. Heating rate: 10°C min^{-1}, in static air. (a) Al_2O_3(Cl, 2); (b) Al_2O_3(Cl, 100); (c) Al_2O_3(N, 2).

Fig. 2. Infrared spectra of $AlCl_3 \cdot 6\,H_2O$, amorphous aluminas and η-Al_2O_3. (a) $AlCl_3 \cdot 6\,H_2O$; (b) Al_2O_3(N, 2); (c) Al_2O_3(Cl, 2); (d) Al_2O_3(Cl, 25); (e) Al_2O_3(Cl, 150); (f) η-Al_2O_3. The η-Al_2O_3 was prepared by the thermal decomposition of $AlCl_3 \cdot 6\,H_2O$ at 850°C for 2 h in flowing air (100 ml min^{-1}).

preparation time. From the fact that no correlation was observed between the surface area and the chlorine content, it is presumed that the chlorine remains mainly in the bulk rather than on the surface of alumina. Al_2O_3(N) gave a smaller surface area (108 $m^2\,g^{-1}$) than Al_2O_3(Cl) and the same density (2.6 g cm^{-3}) as Al_2O_3(Cl). From the SEM observation of Al_2O_3(Cl) and Al_2O_3(N) [part of which is shown in Fig. 8 (a) and (e)] it was found that Al_2O_3(Cl) is the aggregate of thin platelets (<10 μm) and Al_2O_3(N) consists of the block particles of the smooth surface (<15 μm).

Figure 1 shows the TG and DTA curves for Al_2O_3(Cl, 2), Al_2O_3(Cl, 100) and Al_2O_3(N, 2). On heating to 1300°C, the weight loss of 14—20 wt.% was observed for all aluminas. The main part of the loss may be attributable to the dehydration of water present on the surface and in the structure of amorphous aluminas. The presence of water can be confirmed by the IR spectra shown in Fig. 2. In TG curves of Al_2O_3(Cl, 2) and Al_2O_3(Cl, 100), a

small weight decrease appears at around 800°C. This weight loss was accompanied by the evolution of chlorine gas which was detected by test papers of potassium iodide starch. Therefore, the weight loss at 800°C can be accounted for by the liberation of chlorine contained in Al_2O_3(Cl). In fact, the weight losses for Al_2O_3(Cl, 2), Al_2O_3(Cl, 25), Al_2O_3(Cl, 100) and Al_2O_3(Cl, 300) at around 800°C were 2.3, 1.9, 0.8 and 0 wt.%, respectively, and these values, except Al_2O_3(Cl, 2), agree very well with the chlorine content shown in Table 1. Furthermore, an exothermic peak appears in the DTA curve at around 800°C. As the exothermic peak also appears in Al_2O_3(N) which does not contain the chlorine, it is considered that the peak does not correspond to the evolution of chlorine, but to the crystallization of amorphous alumina to η-Al_2O_3, which will be described in Fig. 4.

Figure 2 shows the IR spectra of $AlCl_3 \cdot 6\,H_2O$ and amorphous aluminas. Many absorption bands appear for $AlCl_3 \cdot 6\,H_2O$. Ferraro [5] has reported that OH-stretching and bending vibrations appear at around 3000 and 1620 cm^{-1} and Al—OH bending, rocking, wagging, twisting and Al—O stretching vibrations appear at 1170, 835, 590, 315 and 480 cm^{-1}, respectively. Al_2O_3(Cl) and Al_2O_3(N) give very similar spectra: the large, broad peaks appear at 3400—3500 and 600—800 cm^{-1} and the small peaks at 1620, 1520 and 1420 cm^{-1}. The absorption peaks at 3400—3500 and 1620 cm^{-1} correspond to OH-stretching and bending vibrations as described above. The intensity of the peak at 1520 and 1420 cm^{-1} increases remarkably for the crystalline η-Al_2O_3, which was prepared by the thermal decomposition of $AlCl_3 \cdot 6\,H_2O$ at 850°C for 2 h. Therefore, these peaks may be ascribed to

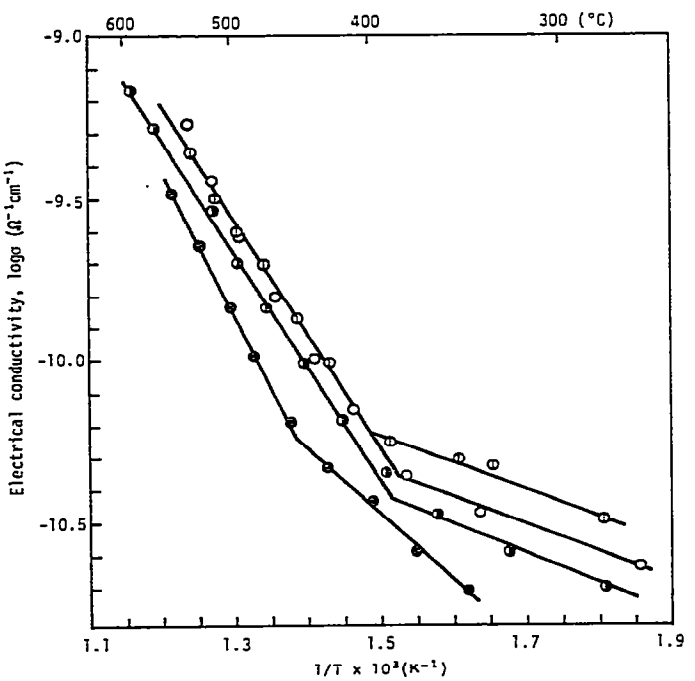

Fig. 3. Variation in electrical conductivity of amorphous aluminas with temperature. ○, Al_2O_3(Cl, 2); ⊙, Al_2O_3(Cl, 25); ◑, Al_2O_3(Cl, 150); ●, Al_2O_3(N, 2).

the Al—O bond. Furthermore, $Al_2O_3(Cl)$ did not give the characteristic absorption peaks of not only the undecomposed $AlCl_3 \cdot 6\,H_2O$, but also of chlorite(ClO_2^-), chlorate(ClO_3^-) and perchlorate(ClO_4^-) [6].

The results in Table 1 and Figs. 1 and 2 can be summarized as follows: (i) the chlorine will be present mainly in the bulk of $Al_2O_3(Cl)$ because of the absence of any interrelation between the chlorine content and the specific surface area (Table 1); (ii) the weight loss with the evolution of chlorine gas (Fig. 1) agrees quite well with the chlorine content shown in Table 1 which was determined by chemical analysis; and (iii) the absorption spectra of ClO_2^-, ClO_3^- and ClO_4^- are not present (Fig. 2). On the basis of this summary, it can be presumed that the chlorine contained in $Al_2O_3(Cl)$ may be present as chloride ion, though it does not give the characteristic IR spectra [6].

Figure 3 shows the electrical conductivity of amorphous aluminas. The measured values of electrical conductivity lie in the range of insulators. The conductivity of $Al_2O_3(Cl)$ tends to decrease with increasing preparation time, but is still higher than that of $Al_2O_3(N)$, probably due to the chlorine contained in $Al_2O_3(Cl)$. Pizzini et al. [7] have found that the electrical conductivity of RuO_2 (exhibits metallic conductivity) obtained by the thermal decomposition of $RuCl_3 \cdot 3\,H_2O$ was similarly influenced by the chlorine content, but the mechanism of the effect is not clear.

Formation of $ZnAl_2O_4$

The reaction behavior and reactivity of $Al_2O_3(Cl)$ and $Al_2O_3(N)$ for $ZnAl_2O_4$ formation have been investigated. Figure 4 shows the results of the DTA experiments for $ZnAl_2O_4$ formation. Curves (a)—(e) are the DTA curves for amorphous alumina alone. The results of X-ray diffraction for the samples quenched from the temperatures shown by the arrows on the DTA curves are also represented in Fig. 4. All samples show two exothermic peaks at 820 and 1080—1170° C. From the results of X-ray diffraction, it is found that the former corresponds to crystallization from amorphous alumina to η-Al_2O_3, and the latter to δ-$Al_2O_3 \rightarrow \alpha$-$Al_2O_3$ in the case of $Al_2O_3(Cl)$ and to η-$Al_2O_3 \rightarrow \theta$-$Al_2O_3 \rightarrow \alpha$-$Al_2O_3$ in $Al_2O_3(N)$. It can therefore be concluded that the transition sequences of amorphous aluminas are $Al_2O_3(Cl) \rightarrow \eta$-$Al_2O_3 \rightarrow \delta$-$Al_2O_3 \rightarrow \alpha$-$Al_2O_3$ and $Al_2O_3(N) \rightarrow \eta$-$Al_2O_3 \rightarrow \theta$-$Al_2O_3 \rightarrow \alpha$-$Al_2O_3$, respectively.

Furthermore, the exothermic peak at around 820° C due to crystallization of $Al_2O_3(Cl)$ tends to become sharp with a decrease in their preparation times; in other words, with an increase in the content of chlorine, while the peak for $Al_2O_3(N)$ is remarkably broad. This tendency can be explained as follows: the larger content of chlorine in $Al_2O_3(Cl)$ results in the more disordered structure and thus the higher rate of crystallization, which leads to a sharp peak. If the oxide ion (ion radius 1.40 Å) in the alumina structure could be replaced by the chloride ion (1.81 Å), the resulting structure should contain the lattice distortion or the cation vacancy. On the other hand, the differences in the temperature and shape of the exothermic peak due to δ-$Al_2O_3 \rightarrow \alpha$-$Al_2O_3$ transformation at about 1170° C are not observed for four $Al_2O_3(Cl)$ samples. This suggests that after the evolution of chlorine the dif-

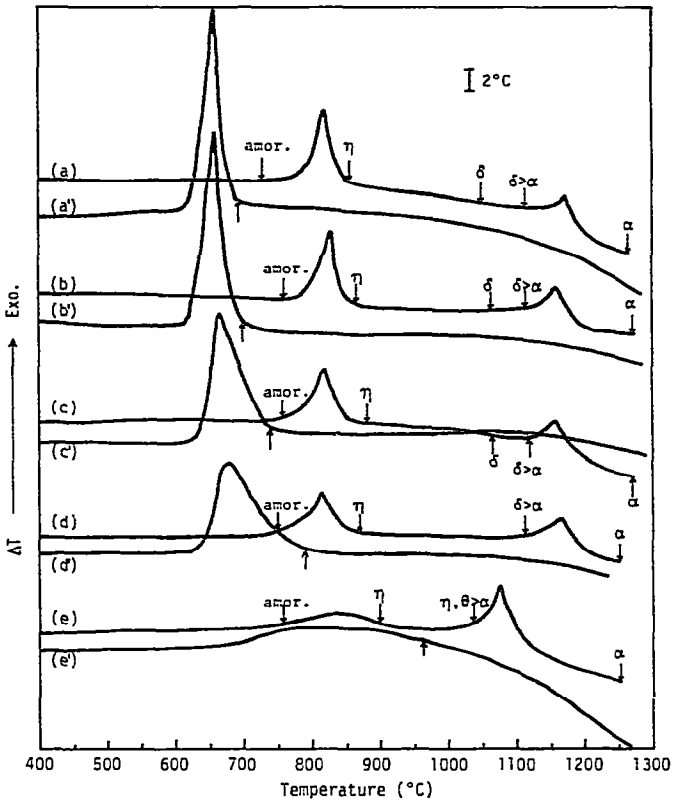

Fig. 4. DTA curves for amorphous aluminas alone and zinc oxide—amorphous alumina mixtures. Heating rate: 10°C min^{-1}, in static air. (a) Al_2O_3(Cl, 2); (a′) ZnO—Al_2O_3(Cl, 2); (b) Al_2O_3(Cl, 5); (b′) ZnO—Al_2O_3(Cl, 5); (c) Al_2O_3(Cl, 25); (c′) ZnO—Al_2O_3(Cl, 25); (d) Al_2O_3(Cl, 150); (d′) ZnO—Al_2O_3(Cl, 150); (e) Al_2O_3(N, 2); (e′) ZnO—Al_2O_3(N, 2).

ference in the structures of aluminas obtained is no longer present. The fact that the temperature of α-transformation of Al_2O_3(N, 2) is lower than that of Al_2O_3(Cl) is probably attributable to the differences in the crystallinity of η-Al_2O_3 crystallized from amorphous aluminas and in the course of transition to α-Al_2O_3.

Curves (a′)—(e′) of Fig. 4 show the DTA curves for the equimolar mixtures of ZnO and Al_2O_3. In contrast to the DTA curves of amorphous aluminas alone, only one exothermic peak appears at around 670° C in ZnO—Al_2O_3(Cl) systems and at around 800° C, though very broad, in the ZnO—Al_2O_3(N) system. After the samples have been quenched from the temperature just after the exothermic peak shown by the arrows on the DTA curves, they were subjected to X-ray diffraction and chemical analysis. In all ZnO—Al_2O_3(Cl) systems, the diffraction lines of $ZnAl_2O_4$ and a trace of the unreacted ZnO were detected, and the fractional formation of $ZnAl_2O_4$(α) was 0.85—0.88. In the ZnO—Al_2O_3(N) system, the lines of $ZnAl_2O_4$ and ZnO were nearly equal in intensities. Furthermore, in Al_2O_3(Cl, 5), Al_2O_3(Cl, 25) and Al_2O_3(Cl, 150) systems, the $ZnAl_2O_4$ formed at the temperatures just after the exothermic peak, i.e., 700, 740 and 790° C, which are shown by the arrows on the DTA curves, had the lattice constant of 8.085 Å and the

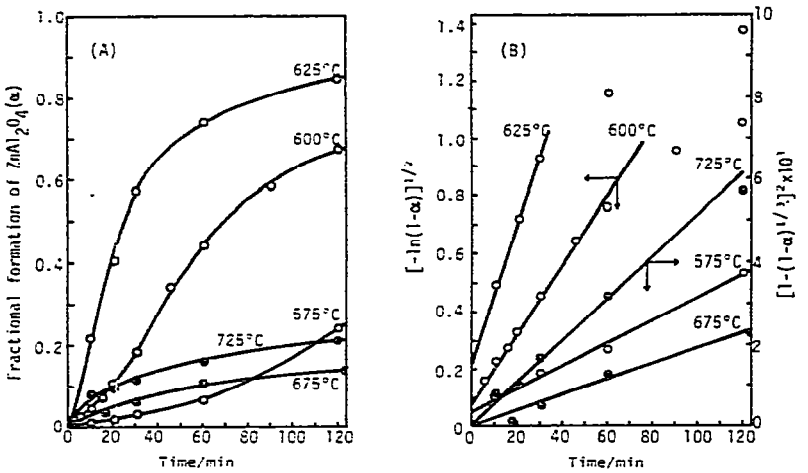

Fig. 5. (A) Rate of $ZnAl_2O_4$ formation at various temperatures. (B) Avrami—Erofeev's and Jander's plots. ○, $ZnO—Al_2O_3$(Cl, 25); ●, $ZnO—Al_2O_3$(N, 2).

crystallite size (D_{440}) of 350, 370 and 390 Å, respectively. From the above results, it is concluded that this exothermic peak corresponds to the formation of $ZnAl_2O_4$ and the reactivity of Al_2O_3(Cl) is higher than Al_2O_3(N). The exothermic peak in $ZnO—Al_2O_3$(Cl) systems tends to become remarkably sharp with decreasing preparation times of Al_2O_3(Cl). This behavior can be explained in the same way as described in the case of crystallization of Al_2O_3(Cl) to η-Al_2O_3, that is, by the more disordered and more reactive alumina structure resulting from an increase in the chlorine content.

Furthermore, in the $ZnO—Al_2O_3$(Cl) systems, the temperature of the exothermic peak due to $ZnAl_2O_4$ formation is lower by ca. 150°C than that of the crystallization of amorphous alumina to η-Al_2O_3. This suggests that Al_2O_3(Cl) in an amorphous state reacts with ZnO. On the other hand, in the $ZnO—Al_2O_3$(N) system, as the temperature range of $ZnAl_2O_4$ formation nearly corresponds to that of the crystallization of Al_2O_3(N), the reaction becomes more complicated. From the difference in the shape of the exothermic peak, i.e., it is sharp in $ZnO—Al_2O_3$(Cl) systems and remarkably broad in the $ZnO—Al_2O_3$(N) system, it can in general be expected that the mechanism of the formation of $ZnAl_2O_4$ differs. The mechanism was therefore further investigated on the basis of the isothermal experiments.

Figure 5 shows the results of isothermal experiments in $ZnO—Al_2O_3$(Cl, 25) and $ZnO—Al_2O_3$(N, 2) systems. As can be seen from Fig. 5(A), the differences in the reaction temperature and the shape of the rate curve are obvious for two reaction systems. As shown in Fig. 5(B), the results in Fig. 5(A) fitted the Avrami—Erofeev equation

$$kt = [-\ln(1-\alpha)]^{1/2} \quad (1)$$

for the $ZnO—Al_2O_3$(Cl, 25) system up to about 0.5 in α, while for the $ZnO—Al_2O_3$(N, 2) system the results fitted the Jander equation

$$kt = [1-(1-\alpha)^{1/3}]^2 \quad (2)$$

The activation energies calculated were 56 kcal mole^{-1} for the $ZnO—Al_2O_3$

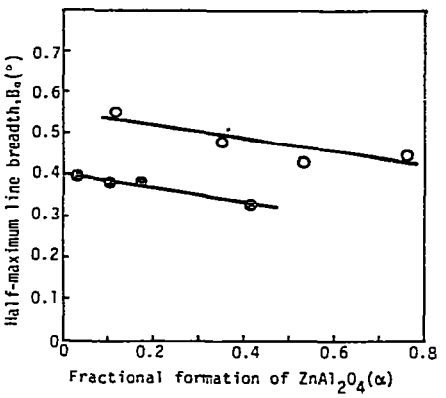

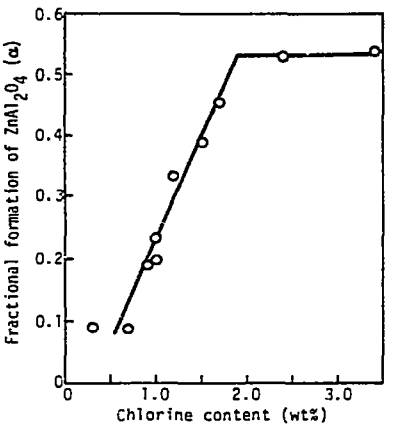

Fig. 6. Variation in half-maximum line breadths of $ZnAl_2O_4$ formed in ZnO—Al_2O_3 Cl, 25) and ZnO—Al_2O_3(N, 2) (●) systems with fractional formation of $ZnAl_2O_4$.

Fig. 7. The influence of the chlorine content in amorphous aluminas (shown in Table 1) on the fractional formation of $ZnAl_2O_4$ formed at 600°C for 1 h.

(Cl, 25) system and 45 kcal mole^{-1} for the ZnO—Al_2O_3(N, 2) system. The results obtained in ZnO—Al_2O_3(Cl, 5) and ZnO—Al_2O_3(Cl, 150) systems also fitted the Avrami—Erofeev equation (not shown in the Fig.). It is considered that such a variation in the kinetics depends not only on the structure and physicochemical properties of amorphous aluminas, but also on those of the $ZnAl_2O_4$ formed. On heating Al_2O_3(Cl, 25) alone at 625°C for 2 h, it was still in an amorphous state, while Al_2O_3(N, 2) transformed to η-Al_2O_3 of poor crystallinity after 2 h at 675°C. This implies that in the ZnO—Al_2O_3(Cl, 25) system, alumina in an amorphous state reacts with ZnO, but in the ZnO—Al_2O_3(N, 2) system, alumina, in which the crystallization to η-Al_2O_3 is in progress, reacts. These results agree with those of DTA experiments shown in Fig. 4. It has been reported previously [8,9] that the reaction of ZnO with the crystalline alumina, e.g., η-, γ-, δ-, θ- or α-Al_2O_3, followed the Jander equation and was controlled by the diffusion of zinc ion through the product layer. In the present study, the fact that the reaction in the ZnO—Al_2O_3(N, 2) system follows the Jander mechanism suggests that alumina in which the crystallization to η-Al_2O_3 is in progress reacts with ZnO and forms the relatively well-crystallized $ZnAl_2O_4$, through which the diffusion of zinc ions becomes rate-determining. On the other hand, the results that the reaction in the ZnO—Al_2O_3(Cl, 25) system follows the mechanism of nucleation growth up to about 0.5 in α may be interpreted on the basis of an assumption that because alumina in an amorphous state reacts with ZnO, $ZnAl_2O_4$ formed has a remarkably disordered structure, through which the diffusion of zinc ions is not rate-determining. In general, the disordered structure as well as the small crystallite size can contribute to X-ray line broadening. Figure 6 shows the plot of the half-maximum line breadth of the D_{511} line of $ZnAl_2O_4$ formed in ZnO—Al_2O_3(Cl, 25) and ZnO—Al_2O_3(N, 2) systems against the fractional formation of $ZnAl_2O_4$(α). It is observed that $ZnAl_2O_4$ obtained from the ZnO—Al_2O_3(Cl, 25) system has a larger line breadth than

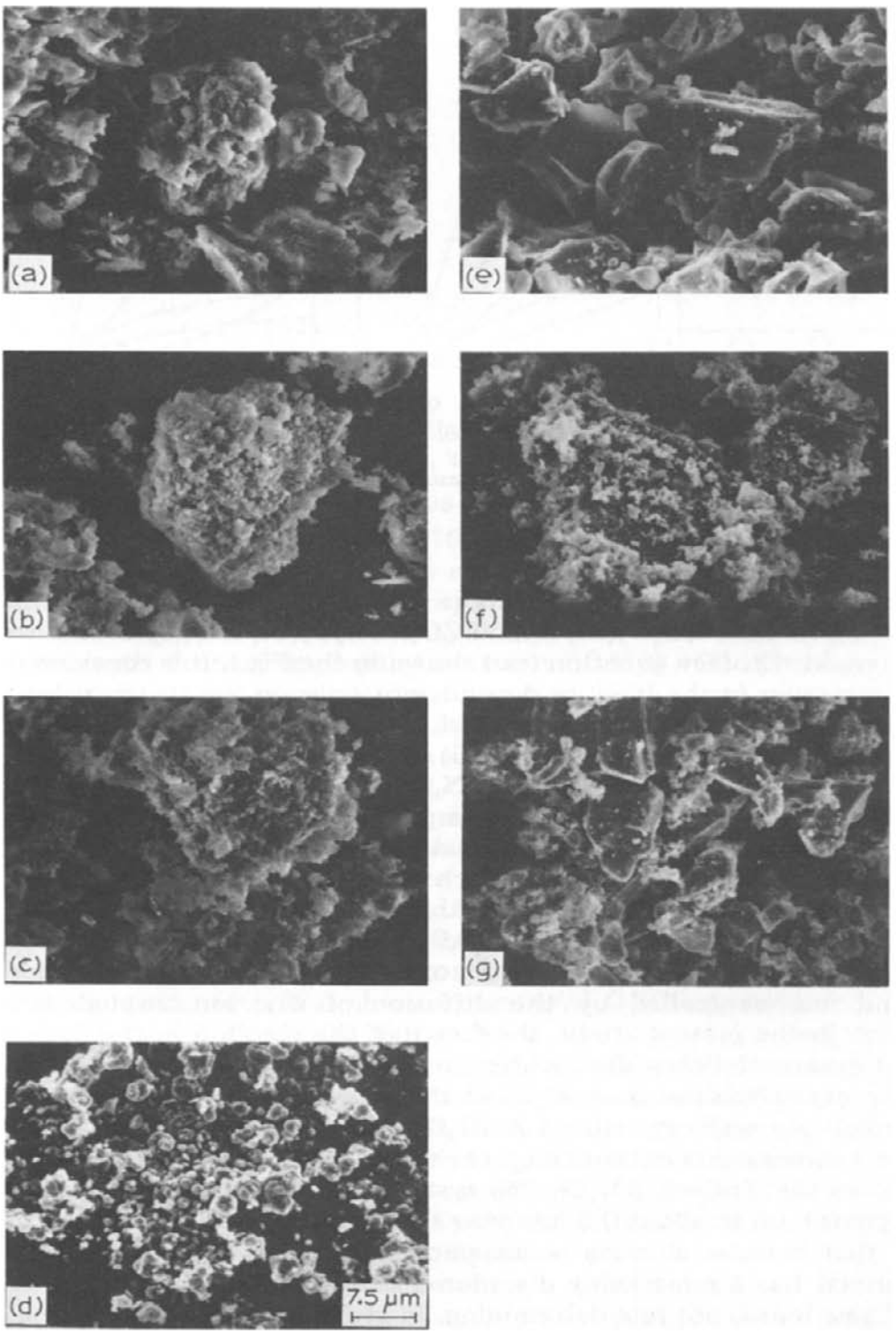

Fig. 8. Scanning electron micrographs of amorphous aluminas, zinc oxide and their mixtures. (a) Al_2O_3(Cl, 25); (b) ZnO—Al_2O_3(Cl, 25), before reaction; (c) ZnO—Al_2O_3(Cl, 25), after reaction at 600°C for 1 h (α = 0.4); (d) ZnO; (e) Al_2O_3(N, 2); (f) ZnO—Al_2O_3 (N, 2), before reaction; (g) ZnO—Al_2O_3(N, 2), after reaction at 800°C for 2 h (α = 0.4).

that from the $ZnO—Al_2O_3$(N, 2) system. This result shown in Fig. 6 may support the assumption described above, if the half-maximum line breadth is allowed to be taken as a measure of the degree of disorder of $ZnAl_2O_4$. Furthermore, the half-maximum line breadth tends to decrease with increasing α-values. This may indicate a decrease in the degree of disorder of $ZnAl_2O_4$ formed as the reaction progresses. It is considered that this decrease is probably correlated with the deviation of data above $\alpha = 0.5$ shown for curves of 600 and 625°C in Fig. 5(B); that is, the transition of the reaction mechanism from the nucleation-growth to the diffusion-control seems to occur as a result of a decrease in the degree of disorder of $ZnAl_2O_4$.

From the results in Figs. 4—6, it is concluded that Al_2O_3(Cl) gives the higher reactivity than Al_2O_3(N), because it has not only the smaller particle size and the higher surface area, but also the disordered structure containing the chlorine and, in addition, reacts in an amorphous state with ZnO. It is expected that the disordered structure and reactivity of Al_2O_3(Cl) are influenced by the chlorine content.

Figure 7 shows the plot of the chlorine content vs. the fractional formation of $ZnAl_2O_4(\alpha)$ measured when ZnO was allowed to react with various Al_2O_3(Cl) shown in Table 1 at 600°C for 1 h. A good linear relationship exists between the α-values and the chlorine content below about 1.8 wt.% and the rate of $ZnAl_2O_4$ formation apparently increases with chlorine content.

Figure 8 shows the scanning electron micrographs of amorphous aluminas, zinc oxide and their mixtures before and after the reaction ($\alpha = 0.4$). Al_2O_3(Cl, 25) in Fig. 8 (a) shows the presence of aggregates of thin platelets (<10 μm). Similar aggregates were observed for other Al_2O_3(Cl) samples having the longer preparation times. Al_2O_3(N, 2) in Fig. 8(e) shows the block particles (<15 μm) of the smooth surface. Zinc oxide in Fig. 8(d) consists of the spherical particles of a few μm or below. From the micrographs of the mixture before the reaction [Fig. 8(b) and (f)], it can be seen that the particles of alumina are well covered with zinc oxide particles. After the reaction [Fig. 8 (g)], the particles of zinc oxide almost disappeared and the surface of Al_2O_3(N, 2) again became smooth in the same manner as before the reaction. This implies that the surface of Al_2O_3(N, 2) was well covered with the product layer of $ZnAl_2O_4$, and thus zinc oxide is the diffusion component. On the other hand, for the $ZnO—Al_2O_3$(Cl, 25) system which follows the nucleation-growth mechanism, the information supporting the mechanism was not obtained from SEM observation, because Fig. 8 (b) and (c) did not allow differentiation between the packing structure of reacting particles before and after the reaction.

REFERENCES

1 T. Tsuchida, M. Kondo, R. Furuichi and T. Ishii, Nippon Kagaku Kaishi, (1974) 1443.
2 T. Sato, F. Ozawa and S. Ikoma, J. Appl. Chem. Biotechnol., 28 (1978) 811.
3 K. Funaki and Y. Shimizu, Kogyo Kagaku Zasshi, 62 (1959) 788.
4 A. Tomonari, Nippon Kagaku Kaishi, 83 (1962) 693.

5 J.R. Ferraro, Low Frequency Vibrations of Inorganic and Coordination Compounds, Plenum Press, New York, 1971, p. 57.
6 R.A. Nyquist and R.O. Kagel, Infrared Spectra of Inorganic Compounds, Academic Press, New York, 1971, p. 14.
7 S. Pizzini, G. Buzzanca, C. Mari, L. Rossi and S. Torchio, Mater. Res. Bull., 7 (1972) 449.
8 T. Tsuchida, R. Furuichi and T. Ishii, Z. Anorg. Allg. Chem., 415 (1975) 175; 423 (1976) 180.
9 D.L. Branson, J. Am. Ceram. Soc., 48 (1965) 591.